Proceedings of International Structural Engineering and Construction, 7(2), 2020
Emerging Technologies and Sustainability Principles
Edited by Askarinejad, H., Yazdani, S., and Singh, A.

ISSN: 2644-108X
www.doi.org/10.14455/ISEC.2020.7(2).STR-28

NONLINEAR FINITE ELEMENT MODELING OF POST-TENSION RC AND RC BEAMS STRENGTHENED WITH NSM FRP RODS

BELAL ELHAROUNEY[1], AYMAN HUSSEIN[1], EZZ EL-DEEN MOSTAFA[1], and AMR EL-NEMR[2]

[1]*Dept of Structural Engineering, Ain Shams University, Cairo, Egypt*
[2]*Dept of Structural Engineering, German University, Cairo, Egypt*

The post-tensioned (PT) reinforced beams can provide a fast construction advantage through precast and cast-in-situ structural elements. However, due to the excessive increase in load capacity, especially when it comes to girder of bridges, the strengthening using Fiber-reinforced polymer (FRP) might be a solution. Near-surface mounted (NSM) is one of the methods used in strengthening cases, especially in the case of non-degraded concrete cover. Furthermore, very few researchers visited this area experimentally, which consider cost-effective. In this paper, two finite element models using the Abaqus program validated experimental results for both Post-tension beam and strengthening of the beam using NSM separately as preliminary models for combining both systems. PT reinforced concrete beam subjected to four-point bending loading as well as reinforced concrete beam strengthened with NSM using FRP bars subjected to two-point bending loading examined and validated through a 3D non-linear finite element (FE) model to be compared by the experimental results. This FE model considered the non-linear constitutive properties of concrete, yielding of steel, and the bond between strand, concrete, and FRP bars at NSM. The models were targeting the strengthening of existing Post tension girder beams of existing bridges structures. These modeling results showed a reasonable agreement with the tested beam results in terms of failure modes, the load capacity, load-deflection curve, and cracking behavior.

Keywords: Pre-stressed, Serviceability, Reinforced concrete, FRP bars.

1 FINITE ELEMENT PROGRAM

Two experimental programs selected to justify against the FE (Finite Element) models developed for Post-tensioned beams and rebar Near-Surface Mounted (NSM) using carbon fiber reinforced polymer (CFRP) bar for further extending the modeling program by combining the two systems. Al-Mahmoud *et al.* (2010) studied the flexural behavior experimentally of reinforced concrete (RC) beams strengthened by the NSM system using CFRP rods. The experimental program includes 3 rectangular cross-section beams dimensioned 150 mm in width and 280 mm in depth with a span of 3 m. Two 12 mm in diameter, deformed bars were used as tension reinforcement with yield strength and elastic modulus of 600 MPa and 210 GPa. The stirrups diameter was 6 mm, with spacing at 150 mm.

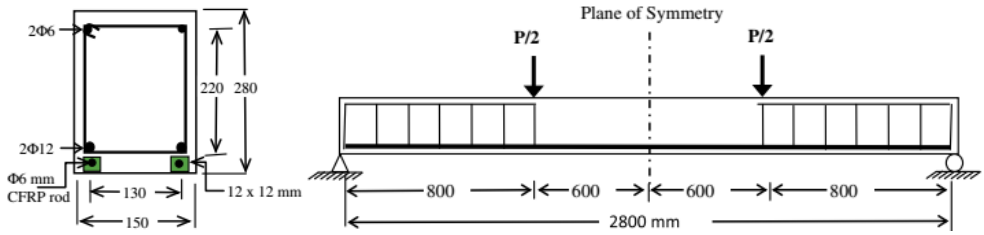

Figure 1. Experimental setup and beam details by Al-Mahmoud *et al.* (2010).

The elastic modulus adopted in the FE model for both concrete and resin was 30.4 and 4.94 GPa. The tensile strength and elastic modulus of the CFRP rods were 1875 MPa and 145.9 GPa. Figure 1 shows the dimensions and reinforcement details of the beams.

The second investigation by Mattock *et al*. (1971) in which supported rectangular-cross-section post-tension reinforced concrete beam with 8.53 m spans examined to explore its flexural behavior. Load capacity, deflection, and cracking behavior were reported. One specimen, RB1, was adopted here in this study. The specimen (RB1) included grout-bonded PT tendons inside the corrugated ducts and the beam pre-stressed by two 1/2 in (12.7 mm) grade 270 seven-wire strands. The tendons draped in the parabolic curve at mid-span 254 mm depth and zeroed eccentricity at the beam supports. Figure 2 shows the details of reinforcement for beam RB1. The tensile strength of concrete, steel bars of diameter 6, and 10 mm were 3.33, 388, and 350 MPa. The elastic moduli for concrete and steel reinforcement were 20, and 200 GPa. Finally, the concrete compressive strength was 28 MPa.

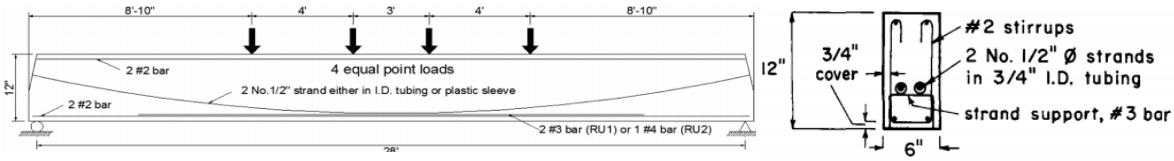

Figure 2. Experimental setup and details for beam (RB1) details (Mattock *et al.* 1971).

2 MATERIAL MODEL

2.1 Uniaxial Behavior of Plain Concrete

A concrete damage plasticity model from several other models existing inside the Abaqus software library adopted to model the concrete beam. In this, the model, the concrete dilation angle valued 45˚ for the RC beams, while the other parameters such as eccentricity, the ratio of biaxial to uniaxial state strengths (f_{b0}/f_{c0}), the ratio of the distance between the hydrostatic axis to deviatoric cross-section (K), and viscosity parameter defined as recommended by the Abaqus manual (2016). The compressive concrete strength used in this research was 30 MPa; however, the stress-strain curve was defined as per Eurocode 2 (2004). Figure 3 shows the compressive stress-strain curve for concrete material used in this model. Kmiecik and Kaminski (2011) developed a tension-stiffening model present in Eq. (1) to simulate the interaction between the concrete and the deformed bars when cracking occurs. The Equation was as follow:

$$\sigma^{(2)}{}_t = f'_t\left(\frac{\varepsilon_{cr}}{\varepsilon_t}\right)^n \text{ for } \varepsilon_t > \varepsilon_{cr} \quad (1)$$

The value of n defined by 1.5 for this study. Figure 4 shows the tension-stiffening model adopted in this FE model for the relationship between concrete and steel reinforcement.

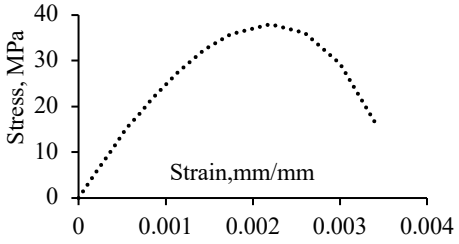

Figure 3. Compressive stress-strain relation of concrete.

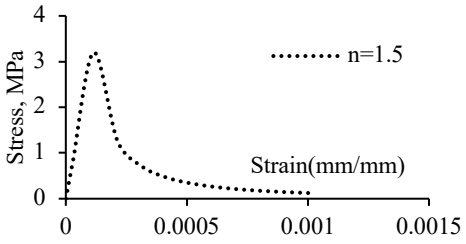

Figure 4. Tension stiffening relationship.

The typical post-tensioned (PT) beam element has a lower reinforcing ratio than conventional RC structures. Hence, the tension-stiffening model should change as the tensile stress drops to the residual stress at a strain of about two times that at cracking. Figure 5 shows the tension-stiffening curve used in FEM for conventional steel reinforcing bars embedded while PT RC beams.

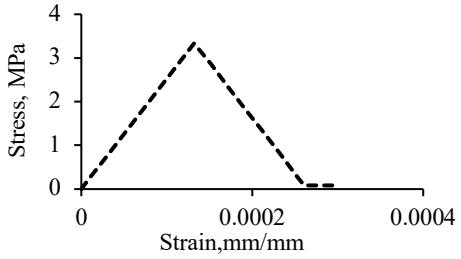

Figure 5. Tension stiffening of conventional steel bars inside the PT RC beams.

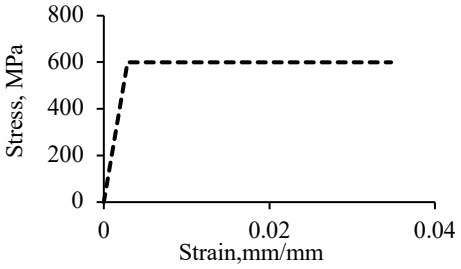

Figure 6. The stress-strain curve of conventional bars used inside PT beam (S-C6 (270-R)).

2.2 Uniaxial Behavior of Steel Reinforcement and Pre-Stressing Tendons

The steel reinforcement modeled using a bi-linear elastic, perfect plastic model. Figure 6 shows the stress-strain relationship used in the FE model for conventional reinforced concrete beam (S-C6 (270-R)). Figure 7 represents the stress-strain curve for steel reinforcement used in the pre-stressing beam (RB1). Devalapura and Tadros (1992) developed a model for the Pre-stressing steel tendons (PT) adopted in the FE model in this study for grade 270 seven-wire strands. The model is a non-linear empirical stress-strain relationship, as shown in Figure 8.

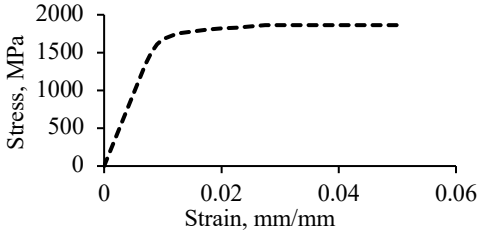

Figure 7. The stress-strain curve of conventional steel bars for conventional RC beam (RB1).

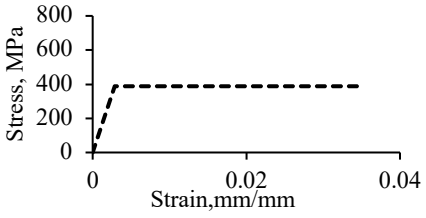

Figure 8. The stress-strain curve of pre-stressing steel.

2.3 Uniaxial Behavior of FRP Rods and Epoxy Adhesive

The tensile behavior of the CFRP bar is linear up to its ultimate tensile strength, as represented in Figure 9. After ultimate tensile strain, ε_{fu}, the contribution of the CFRP bars neglected. The elastic-perfectly plastic stress-strain diagram represented in Figure 10 is used to simulate the tensile behavior of the epoxy adhesive.

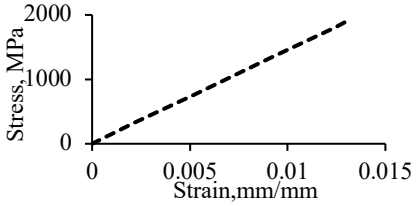

Figure 9. The tensile stress-strain curve of CFRP bar.

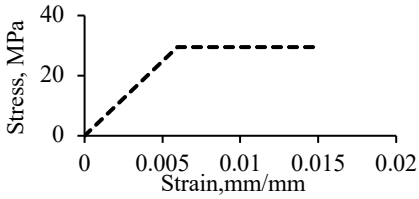

Figure 10. The tensile stress-strain curve of epoxy.

3 INTERACTION BETWEEN PARTS

The bond between steel reinforcement and concrete is assumed as a perfect bond. The loading plates and the supporting plates were simulated through a tie constraint mechanism to the RC beam. The interaction between the interior steel reinforcement and the concrete beam as well as the interaction between the FRP rod and the Epoxy resin simulated using the embedded element constraint. Surface-to-surface contact pairs assigned to the concrete-epoxy interface using a cohesive zone model for presenting the cohesion between the concrete surface and epoxy. The tensile resistance at the concrete-epoxy interface assumed the tensile capacity of the weakest material in which the concrete tensile strength presented in Eq. (2)

$$\sigma_{max} = 0.6\sqrt{f'_c} \tag{2}$$

Hence, the debonding was assigned to occur at the concrete epoxy interface when modeling the NSM CFRP bars. The cohesive zone model starts initially with an increasing segment up to the ultimate shear stress (τ_{max}) and its corresponding slip (δ_u) and then continues with a softening behavior up to the ultimate slip, which assumed to be four times the slip corresponding to that at ultimate shear stress (Hawileh 2012). The value of τ_{max} for the model obtained using Eq. (3), as Hassan (2002) suggested in the case of round deformed bars.

$$\tau_{max(epoxy-concrete)} = \frac{f_{ct}\mu}{G_1} \tag{3}$$

Hence, in Eq. (3), the μ valued by 1 as proposed by De Lorenzis and Teng (2007) and Hibbitt *et al.* (2016). G_1 is a coefficient determined using a finite element analysis proposed by Hassan (2002), which values the G_1 by 0.65. The initiation of damage is assumed to occur at nominal stress ratios of one, which is a function of the maximum contact stress value. Thus, when the separation is normal to the interface or in the first or the second shear direction, the slip occurs till the concrete surface – epoxy interface occurs. Several parameters in Abaqus while modeling explains this behavior. For remodeling purposes, the values of $G^n{}_s, G^c{}_t, and\ G^c{}_s$ parameters were evaluated by 0.086 N/mm, 1.083 N/mm, and 1, respectively. The interaction between tendon and concrete modeled using a contact formulation surface-to-surface contact in Abaqus/standard contact formulations and Multi-Point Constrains (MPCs) provided in Abaqus (for rigid beam) constraint to simulate the anchorage zone.

4 MESH CONFIGURATION, LOADING, AND BOUNDARY CONDITIONS

Meshing configuration is one function in FE modeling. Hence, the beam S-C6 (270-R) meshing was refined at a specific location where relatively high strain gradients expected to take place. Similarly, the meshing generation developed using the same techniques for 2 models. Unnecessary refining is neglected for computational time consumption purposes such as the outer zone of the groove. The fine mesh is used inside the strengthening groove to increase the accuracy of the results. Concrete Part and Epoxy modeled using (C3D8R) element with a maximum element mesh size of 50 mm. The conventional steel bars and FRP bars modeled using (T3D2) with an approximate maximum element mesh size of 25 mm. Similar procedures are considered when modeling beam (RB1). The pre-stressing steel tendon modeled as solid elements (C3D6R) with an approximate maximum element size of 50 mm. The mesh technique was sweep meshing. The loading condition was simulated by a load control distributed type over two loading areas selected at the general step. In the Pre-stressing model, load control was implemented at four reference points tied by a couple constrained to four loading plates. The load control is applied as a second step after the post-tension step in ramp form, which applies the load in linear increments. The pre-stressing applied in tendons valued by 1298.5 N/mm^{2,} similar to the tested beam. While boundary condition was assigned at the centerline nodes of the left support plate in which translation in X, Y, and Z-directions are restrained (i.e., hinged support). Similarly, the centerline nodes of the right support plate restrained from the translation in Y-direction only (i.e., roller support). Consequently, the same procedure followed while the boundary conditioning beam (RB1).

5 FINITE ELEMENT MODEL RESULTS

Figures 11 and 12 illustrate failure modes, the crack pattern for beams S-C 6 (270-R) and (RB1).

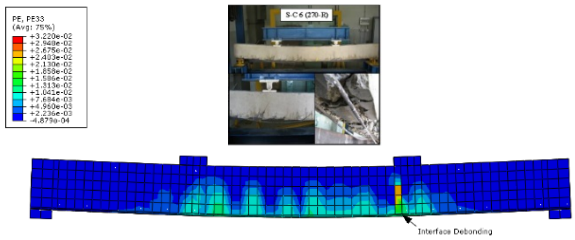

Figure 11. The crack pattern for beam S-C 6 (270-R).

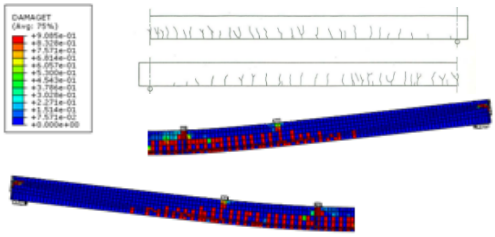

Figure 12. The crack pattern for beam (RB1).

As shown from Figures 11 and 12, the FE model provides a proper agreement in terms of crack patterns with the experimental test results, including the crack spacing. Furthermore, a comparison was held between the load-deflection curve obtained from the experimental tests and those from FE models, as shown in Figure 13 (a and b). As shown from Figure 13 (a and b), the 2 FE models established to simulate the beam S-C 6 (270-R) and (RB1) provided an entirely accurate agreement with the load-deflection curve till the failure load capacity that the beams can handle. Table 1 provides the error between the experimental and FE models for the ultimate load at failure resulted. From Table 1, the accuracy of the ultimate load capacity validated providing a value of 14.4 and 9.8% between the experimental test results and those results obtained from FE models, which means good accuracy can achieve when using these models for further combing them to handle experimental FE program for strengthening the Post-tensioning RC beams.

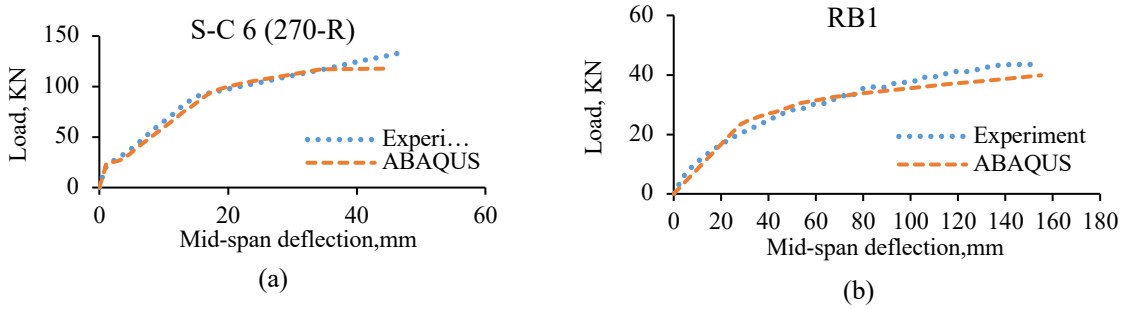

Figure 13. Load-deflection curve of tested and FE modeled beams (a) S-C 6 (270-R), and (b) (RB1).

Table 1. Comparison between the experimental and FE model results in terms of ultimate load at failure.

Beam	Experimental, (KN)	FEM ABAQUS, (KN)	FEM ABAQUS/ Experimental
S-C 6 (270-R)	134.2	117.3	-14.4%
(RB1)	43.63	39.85	-9.48%

6 CONCLUSION

This study aims to validate the accuracy of 2 FE models generated for predicting the load capacity and the load-deflection curve of PT RC beams and RC beam strengthened with NSM FRP. The FE modeling technique showed a successful simulation for the geometry, material properties, loading, and restraint boundary conditions of the tested beams. The accuracy of the load capacity provided 85.6 and 90.2% between the experimental and the 2 FE models results. A good accuracy anticipated when combing these models to handle the FE program for strengthening the PT RC beams.

References

Al-Mahmoud F., Castel A., François R., and Tourneur C. R. C., *Beams Strengthened with NSM CFRP Rods and Modeling of Peeling-Off Failure*, Composite Structures, 92(8), 1920–30, 2010.

De Lorenzis L., and Teng J. G., *Near-Surface Mounted FRP Reinforcement: An Emerging Technique for Strengthening Structures*, Composites-Part B, 38, 119–43, 2007.

Devalapura, R. K., and Tadros, M. K., *Critical Assessment of ACI 318 Eq. (18-3) for Prestressing Steel Stress at Ultimate Flexure*, ACI Structural Journal, 89(5), Sept.-Oct., 538-546, 1992.

Eurocode 2, Design of Concrete Structures. Part 1-1: General Rules and Rules for Buildings, 2004.

Hassan, T., *Flexural Performance and Bond Characteristics of FRP Strengthening Techniques for Concrete Structures,* PhD Thesis, University of Manitoba, Winnipeg, Canada, 2002.

Hawileh, R. A., *Non-Linear Finite Element Modeling of RC Beams Strengthened with NSM FRP Rods, Construction and Building Materials,* 27(1), 461-471, 2012.

Hibbitt, H. D., Karlsson, B. I., and Sorensen, P., *ABAQUS: Theory Manual,* Providence, Hibbitt, Karlsson and Sorensen, 2016.

Kmiecik P., and Kamiński M., *Modelling of Reinforced Concrete Structures and Composite Structures with Concrete Strength Degradation Taken into Consideration*, Archives of Civil and Mechanical Engineering, 11(3), 623-636, 2011.

Mattock, A. H., Yamazaki, J., and Kattula, B. T., *Comparative Study of Pre-Stressed Concrete Beams, With and Without Bond,* ACI Journal Proceedings, 68(2), Feb., 116-125, 1971.